


Filtered strong quantum correlation of resonance fluorescence from a two-atom radiating system with interatomic coherence

Ze-an Peng,¹ Guo-qing Yang,² Qing-lin Wu,¹ and Gao-xiang Li^{1,*}

¹*Department of Physics, Huazhong Normal University, Wuhan 430079, China*

²*College of Electronics and Information, Hangzhou Dianzi University, Hangzhou 310018, China*

 (Received 4 December 2018; revised manuscript received 16 February 2019; published 11 March 2019)

Frequency-resolved quantum correlation of resonance fluorescence is investigated in a two-atom radiating system. In this quantum radiating system, only one atom is driven by a laser field, and the spontaneous transition of the undriven atom resonates with one of the Rabi sidebands of the driven atom. A single-mode empty cavity is applied to serve as a Lorentzian filter to output the superbunched fluorescent photon pairs when its frequency is tuned to halfway between the central peak and one of the side peaks. In the case of large filter width, two-photon correlation signal and its physical correspondence can be bridged analytically in our approach. It reveals that this superbunching effect turns out to be the constructive quantum interference between a pair of coupled two-photon cascaded transitions. Ulteriorly, it is the consequence of the modulations of the unfiltered dressed-state transition amplitudes by the filter. Our analytical formalism also shows that, although the dipole-dipole interaction is usually weak, the interatomic coherence caused by this weak perturbation can also play a crucial role in breaking through the superbunching limit obtained from a single two-level atom in the same parameter regime. In addition to being a treasurable quantum pump to probe into the target quantum system, it is also found in our investigation that this superbunched fluorescence can serve as a promising quantum response in detecting this weak perturbation in the interior of the quantum source. A general case is also considered when the two-atom radiating system is monitored by two filter-detector monitoring systems. It is found that this filtered strong quantum correlation can be maintained even though the two photons are spatially separated.

DOI: [10.1103/PhysRevA.99.033819](https://doi.org/10.1103/PhysRevA.99.033819)

I. INTRODUCTION

With the frequency filtering and engineering techniques gradually opening up a promising perspective for resonance fluorescence [1–5] and cavity-quantum electrodynamics [6,7], frequency-resolved quantum correlation has attracted considerable attention in recent years. On the one hand, as a treasurable source of correlated photons, frequency-resolved resonance fluorescence deeply reveals the underlying physical scenario of quantum emitter radiating photons in frequency and time domains [8–14]. On the other hand, it also serves as a promising quantum excitation from a quantum light source to drive another target quantum system [15,16], triggering a burgeoning field called “Mollow spectroscopy” [17]. Recently, an inconspicuousness in Mollow spectroscopy has been excavated that superbunching effect can be achieved from halfway between the central peak and each side peak in Mollow spectrum [8,17]. This effect is attributed to the leapfrog transitions involving virtual states [8,18] or the frequency postselection [19]. Undoubtedly, the superbunched fluorescence built up from this mechanism carries considerable potential applications. For example, it can not only provide a highly sensitive quantum signal in detecting weak interaction between light and atoms [17,20], but also serve as a popular quantum entanglement source to prepare strong correlated photon pairs. Recently, it has been verified

experimentally that this frequency-resolved strong correlated photon pair is able to violate the Cauchy-Schwarz inequality and Bell’s inequality [21–23].

However, in order to output the filtered fluorescence with the desired frequency, how to tackle the frequency filtering theoretically is also another main topic. The complete and primitive description of filtering process requires that the original fluorescent filed operator $E(t)$ of the quantum radiating source should be dressed into the filtered filed operator $E_f(t)$ by the filtering function as $E_f(t) = \int_0^\infty f(\lambda, \omega_f, \tau)E(t - \tau)d\tau$ [24–26] with λ and ω_f being the filter pass-band width and filter setting frequency. However, unfortunately, this exquisite description may also lead to extensive considerations of time orderings and mathematical complexity. Concerned with this topic, del Valle *et al.* have carried on a systematic research and proposed a pioneering sensors method in weak coupling regime between quantum emitter and sensors [27]. On the one hand, this weak coupling regime is, physically, to eliminate the reactions of the filter to the quantum emitter, retaining only the incident effects of the emitted photons on the filter [26,28]. In this respect, it can be considered as a unidirectional interaction from the emitter to the filter, structuring a cascaded quantum system [29,30]. On the other hand, because the pass-band width of the filter characterizes its average resolution ability [31], a Lorentzian filter can be replaced physically by a such single-mode quantum empty cavity that its decay rate and resonance frequency, respectively, correspond to the pass-band width and setting frequency of the filter.

*gaox@mail.ccnu.edu.cn

Based on these two points, in this theoretical work, we employ a quantum cascade approach to investigate the frequency-resolved superbunching effect in a two-atom radiating system with the aim of exploring the underlying applications of this strong quantum correlation in the collective atomic system. Compared with a single atom, more steerable geometrical factors including the geometrical configuration and detection azimuth can be controlled in a multiatom system [32]. In our two-atom radiating system, only one atom is driven by an external laser field, and the spontaneous transition of the undriven atom resonates with one of the Rabi side peaks of the former. Resonance fluorescence is injected into a cavity unidirectionally, and the superbunched photon pairs can be outputted when the cavity frequency is tuned to halfway between the central peak and one of the side peaks. In general, the dipole-dipole interaction is not important as long as the interatomic spacing is not extremely small [33,34]. Therefore, this weak interaction and sideband resonance condition ensure that the shape of the host atom's Mollow triplet may not be greatly deformed by the incorporation of the guest atom. Therefore, it can keep the strong quantum correlation from being destroyed. However, on the contrary, it is found that the degree of the two-photon correlation can be enhanced to break through the superbunching limit in a single two-level atom via the interatomic coherence under the same conditions. Apart from that, it can also sensitively response the weak variation of the interatomic distance. This application indicates that, in addition to being a treasure quantum pump to probe into the target quantum system, this strongly correlated fluorescence may also be an excellent response to characterize the internal perturbation of the quantum source itself.

For another purpose, in the limit of large pass-band width, we examine the physical mechanism of this strong quantum statistics analytically from the perspective of conditional detection [35–38]. In the case of filter-target spectral band resonant detection for the central peak and a side peak, destructive quantum interference between a pair of coupled two-photon cascaded channels with opposite emission orderings gives rise to the antibunching effect [10–12]. However, compared with this resonant case, it is found from our investigation that the superbunching effect turns out to be the consequence of constructive quantum interference. Interestingly, this mechanism can be revealed transparently from our analytical approach presented in this paper.

The outline of this paper is organized as follows. In Sec. II, the cascaded quantum system under our consideration is described. In Sec. III, in the limit of large filter width, analytical investigation for the stationary two-photon correlation of the filtered fields is carried out from the conditional state. Correspondingly, the physical mechanism of the fluorescent radiations, especially the superbunching effect, is revealed transparently. Section IV is devoted to discuss the applications of this two-atom system in enhancing the superbunching effect and precisely detecting the variation of the interatomic distance. In Sec. V, a general case is also discussed in which the filtered strong quantum correlation is resolved by two filter-detector monitoring systems. Finally, a conclusion is presented in Sec. VI.

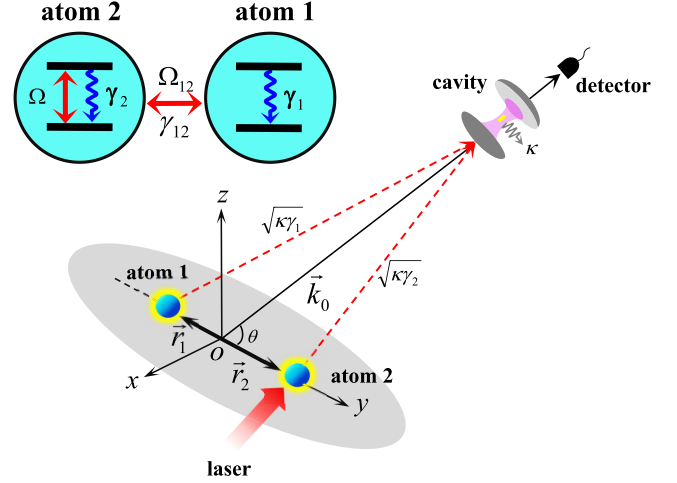


FIG. 1. Schematic diagram of the cascaded quantum system comprising the two-atom quantum radiating source and a filter-detector monitoring system. Collective resonance fluorescence with propagation vector \vec{k}_0 is injected into a single-mode cavity to achieve the strong quantum correlation when the cavity frequency is tuned to halfway between the central peak and one of the side peaks. $\sqrt{\kappa\gamma_i}$ ($i = 1, 2$) are the dissipative coupling strengths between the i th atom and the target cavity, and θ is the observation angle.

II. CASCADED QUANTUM SYSTEM

We first consider a simple configuration, in which the quantum radiating source is monitored by a single photodetector with position vector \vec{R} , as sketched in Fig. 1. In this cascaded configuration, the quantum radiating system is composed of two two-level atoms with excited states $|e_i\rangle$ and ground states $|g_i\rangle$ ($i = 1, 2$), spatially separated by a distance $r_{12} = |\vec{r}_2 - \vec{r}_1|$. The host atom (labeled by atom 2) is driven by a classical laser field with frequency ω_l . At the same time, the host atom is also coupled with a guest atom (labeled by atom 1) via the dipole-dipole interaction. A single-mode frequency-tunable empty cavity of frequency ω_c is applied to serve as a Lorentzian filter. Therefore, it is activated unidirectionally by the resonance fluorescence radiated from the laser-driven quantum radiating system.

In the frame rotating of driving frequency and in the dipole approximation, the dynamical evolution of the total cascaded quantum system, described by the density operator ρ , is dominated by the master equation [33,39–41]

$$\frac{d\rho}{dt} = -\frac{i}{\hbar}[H, \rho] + \mathcal{L}_C\rho + \mathcal{L}_A\rho + \mathcal{L}_{12}\rho + \mathcal{L}_{AC}\rho. \quad (1)$$

The original Hamiltonian of the total system in Eq. (1) takes the form of

$$H = \sum_{i=1,2} \hbar \frac{\Delta_i}{2} \sigma_z^{(i)} + \hbar \Delta_c a^\dagger a + \hbar \frac{\Omega}{2} (\sigma_+^{(2)} + \sigma_-^{(2)}) + \hbar \Omega_{12} (\sigma_+^{(1)} \sigma_-^{(2)} + \sigma_+^{(2)} \sigma_-^{(1)}), \quad (2)$$

where $\Delta_i = \omega_{eg}^{(i)} - \omega_l$ and $\Delta_c = \omega_c - \omega_l$ are, respectively, the detunings of the i th atomic frequency $\omega_{eg}^{(i)}$ and the cavity resonance frequency ω_c with respect to the driving frequency ω_l . The third term of the Hamiltonian describes the dipolar

interaction between the host atom and the classical driving field with Rabi frequency Ω . The last term of the Hamiltonian represents the coherent dipole-dipole interaction between the two atoms with strength Ω_{12} . In addition, the operators $\sigma_+^{(i)} = |e_i\rangle\langle g_i|$ and $\sigma_-^{(i)} = |g_i\rangle\langle e_i|$ are the atomic flip operators, and $\sigma_z^{(i)} = |e_i\rangle\langle e_i| - |g_i\rangle\langle g_i|$ is the operator for population inversion. The damping terms in the master equation take the forms of

$$\begin{aligned} \mathcal{L}_C\rho &= \frac{\kappa}{2}\mathcal{L}[a]\rho, & \mathcal{L}_A\rho &= \sum_{i=1,2} \frac{\gamma_i}{2}\mathcal{L}[\sigma_-^{(i)}]\rho, \\ \mathcal{L}_{12}\rho &= -\frac{\gamma_{12}}{2}([\sigma_+^{(1)}, \sigma_-^{(2)}\rho] + [\sigma_+^{(2)}, \sigma_-^{(1)}\rho]) + \text{H.c.}, \\ \mathcal{L}_{AC}\rho &= -\sum_{i=1,2} \sqrt{\kappa\gamma_i}([a^\dagger, \sigma_-^{(i)}\rho]e^{i\vec{k}_0\cdot\vec{r}_i} + \text{H.c.}), \end{aligned} \quad (3)$$

with the Lindblad-type superoperator $\mathcal{L}[\mathcal{O}]\rho = [\mathcal{O}\rho, \mathcal{O}^\dagger] + [\mathcal{O}, \rho\mathcal{O}^\dagger]$. In Eq. (3), $\mathcal{L}_C\rho$ and $\mathcal{L}_A\rho$ represent the dissipations of the target cavity mode and the atomic system to the continuum background modes, respectively. The parameters κ and γ_i are the decay rate of the cavity mode and the spontaneous transition rates of the i th atom, respectively. The third term in Eq. (3), $\mathcal{L}_{12}\rho$, describes the vacuum-induced dissipative coupling between these two atoms via photon exchange with strength γ_{12} [32–34]. The last term, $\mathcal{L}_{AC}\rho$, denotes the unidirectional transmission of fluorescent photons from the quantum source to the target cavity [29,30]. Note that the exponential phase factors play important roles because the atomic emission operator perceived by the detector (or the cavity) in the far-field zone carries a phase difference. The vector \vec{k}_0 is the propagation vector of the fluorescent fields, and we have applied the far-field approximation $|\vec{R} - \vec{r}_i| \approx |\vec{R}| - \vec{e}_R \cdot \vec{r}_i$, where \vec{e}_R is the unit vector in the direction of \vec{R} [32]. The explicit values of γ_{12} and Ω_{12} are determined by the potential energy of dipole-dipole interaction \mathcal{E}_{12} via the relations $\Omega_{12} = \text{Re}[\mathcal{E}_{12}]$ and $\gamma_{12} = -\text{Im}[\mathcal{E}_{12}]$, where [34]

$$\begin{aligned} \mathcal{E}_{12} &= -\frac{3}{2}\sqrt{\gamma_1\gamma_2} \left\{ (1 - \cos^2\Theta) \frac{1}{k_0 r_{12}} \right. \\ &\quad \left. + (1 - 3\cos^2\Theta) \left[\frac{i}{(k_0 r_{12})^2} - \frac{1}{(k_0 r_{12})^3} \right] \right\} e^{ik_0 r_{12}}, \end{aligned} \quad (4)$$

with Θ being the dipole-polarized angle from the interatomic axis, and $k_0 = 2\pi/\lambda_0$ (λ_0 is the radiation wavelength). The symbols ‘‘Re’’ and ‘‘Im’’ denote the real part and imaginary part, respectively.

By working in the strong driving regime, i.e., $\Omega \gg \gamma_1, \gamma_2$, the description of the quantum radiating system is transformed into the dressed two-atom collective representation with the introduction of the dressed two-atom collective bases and the corresponding energies

$$\begin{aligned} |1_A\rangle &= |e_1, +\rangle, & E_1 &= \frac{\hbar}{2}(\bar{\Delta} + \bar{\Omega}), \\ |2_A\rangle &= |e_1, -\rangle, & E_2 &= \frac{\hbar}{2}(\bar{\Delta} - \bar{\Omega}), \\ |3_A\rangle &= |g_1, +\rangle, & E_3 &= -\frac{\hbar}{2}(\bar{\Delta} - \bar{\Omega}), \\ |4_A\rangle &= |g_1, -\rangle, & E_4 &= -\frac{\hbar}{2}(\bar{\Delta} + \bar{\Omega}), \end{aligned} \quad (5)$$

where $|+\rangle = c|e_2\rangle + s|g_2\rangle$, $|-\rangle = s|e_2\rangle - c|g_2\rangle$ are the semiclassical laser-dressed bases of the driven host atom, in which the parameters are $c, s = \sqrt{(\bar{\Omega} \pm \Delta_2)/2\bar{\Omega}}$ with the general Rabi frequency $\bar{\Omega} = \sqrt{\Omega^2 + \Delta_2^2}$. The parameter $\bar{\Delta} = \Delta_1 - \Delta_2$ appearing in the eigenenergies is the detuning between the two atoms’ transition frequencies. In this dressed two-atom collective representation, the emission operators of the bare atoms can be expressed by $\sigma_{ll'} = |l_A\rangle\langle l'_A|$ ($l, l' = 1, 2, 3, 4$), which describes the quantum transition between two levels of two adjacent manifolds of the dressed two-atom collective states. Therefore, the bare emission of atom 1 can be expressed as $\sigma_-^{(1)} = S_1^- = \sigma_{31} + \sigma_{42}$. Whereas, the emission of the driven atom can be decomposed into three parts as $\sigma_-^{(2)} = S_T^- + S_R^- + S_F^-$. The components $S_T^- = -c^2(\sigma_{21} + \sigma_{43})$ and $S_F^- = s^2(\sigma_{12} + \sigma_{34})$ give rise to the higher-frequency side peak of the resonance fluorescence spectrum labeled by ‘‘T’’ and lower-frequency side peak labeled by ‘‘F,’’ respectively. The remaining one $S_R^- = cs(\sigma_{11} + \sigma_{33} - \sigma_{22} - \sigma_{44})$ gives rise to the emission of central peak labeled by ‘‘R’’ at driving frequency.

In order to keep the shape of the Mollow triplet and without loss of generality, we assume that the spontaneous transition of the undriven atom resonates with the higher-frequency Rabi sideband of the laser-driven atom, i.e., $\bar{\Delta} = \bar{\Omega}$. This leads to the near degeneracy between the states $|2_A\rangle$ and $|3_A\rangle$. In this circumstance, we make a second rotating-wave transformation to only drop the fast-rotating terms involving atomic variables. Therefore, the Hamiltonian of the total quantum cascaded system is rewritten in terms of the dressed two-atom collective states as

$$\tilde{H} = \tilde{H}_0 + \tilde{H}_{12}, \quad (6)$$

with the free part and the coherent coupling part

$$\begin{aligned} \tilde{H}_0 &= \hbar\bar{\Omega}(\sigma_{11} - \sigma_{44}) + \hbar\Delta_c a^\dagger a, \\ \tilde{H}_{12} &= -\hbar\Omega_{12}c^2(\sigma_{23} + \sigma_{32}). \end{aligned} \quad (7)$$

The dissipations in Eq. (3) are also transformed as

$$\begin{aligned} \tilde{\mathcal{L}}_C\rho &= \frac{\kappa}{2}\mathcal{L}[a]\rho, & \tilde{\mathcal{L}}_A\rho &= \frac{\gamma_1}{2}\mathcal{L}[S_1^-]\rho + \frac{\gamma_2}{2} \sum_{j=F,R,T} \mathcal{L}[S_j^-]\rho, \\ \tilde{\mathcal{L}}_{12}\rho &= -\frac{\gamma_{12}}{2}([S_1^+, S_T^- \rho] + [S_T^+, S_1^- \rho]) + \text{H.c.}, \\ \tilde{\mathcal{L}}_{AC}\rho &= -\sqrt{\kappa\gamma_1}([a^\dagger, S_1^- \rho]e^{i\vec{k}_0\cdot\vec{r}_1} + \text{H.c.}) \\ &\quad - \sqrt{\kappa\gamma_2} \sum_{j=F,R,T} ([a^\dagger, S_j^- \rho]e^{i\vec{k}_0\cdot\vec{r}_2} + \text{H.c.}). \end{aligned} \quad (8)$$

Note that the original density operator is now transformed as $\tilde{\rho}(t) = e^{i(\tilde{H}_0/\hbar)t} \rho(t) e^{-i(\tilde{H}_0/\hbar)t}$, but it is still labeled by ρ in Eq. (8) and in the following. More noteworthy is that, in our consideration, all the fluorescent peaks are included in the unidirectional radiation into the cavity for completeness, although the cavity mode may be far away from a side peak when it is tuned between the R peak and another side peak. In other words, all the atomic emission operators are not ignored in our consideration. Therefore, the unidirectional dissipative coupling from the atomic system to the cavity in Eq. (8), i.e., $\tilde{\mathcal{L}}_{AC}\rho$, is completely equivalent to its original form $\mathcal{L}_{AC}\rho$ in

Eq. (3) because it is only rewritten in terms of the dressed two-atom collective states. The rotating-wave approximation only treating for atomic variables makes it possible to analytically obtain the atomic populations [34], and its validity will be demonstrated later.

III. CONDITIONAL DETECTION OF FILTERED RESONANCE FLUORESCENCE

In this paper, we are mainly interested in the filtering process with large filter pass-band width specified as $\kappa \gg \gamma_1, \gamma_2$ [10] with the aim of obtaining physically perspicuous results to probe into the radiating mechanism of fluorescent photons. In order to explore the frequency selection of the filter on the fluorescent spectrum, let us focus on the case of $\Omega \gg \kappa$. In this case, the selection effects of the filtering function on each peak band are different that it mainly extracts the photons near the filter setting frequency. In addition, for the sake of simplicity, we assume $\gamma_1 = \gamma_2 = \gamma$ in the following discussion.

Consider the situation that two filtered photons are detected simultaneously. The stationary equal-time two-photon correlation signal of the filtered fluorescence fields is expressed by the operators of the target quantized cavity mode as $g^{(2)} = \langle a^\dagger a^\dagger aa \rangle / \langle a^\dagger a \rangle^2$. The unnormalized two-photon quantum correlation signal, labeled by $G^{(2)}$, can be expressed as $G^{(2)} = \langle a^\dagger a^\dagger aa \rangle = \text{Tr}[a \rho^r a^\dagger]$, where $\rho^r = a \rho a^\dagger$ is the conditional (collapsed) state of the dressed collective atom-cavity system conditioned by detecting a photon [35–38]. In the filtering process, the cavity substituting a Lorentzian filter is assumed to pass through only one fluorescent photon at a time [42]. Therefore, the conditional state ρ^r can be determined in a truncated Hilbert space with single-excitation regime ($|0_a\rangle, |1_a\rangle$). In other words, the collapsed Hilbert space is spanned by the state vectors $|i_A, n_a\rangle$ with $i = 1, 2, 3, 4$ and $n = 0, 1$. Interestingly, after solving the master equation in stationary dynamics, it is found that the conditional state turns out to be a very compact form as

$$\begin{aligned} \rho^r = & \rho_{11}^s |\psi_1\rangle \langle \psi_1| + \rho_{22}^s |\psi_2\rangle \langle \psi_2| + \rho_{33}^s |\psi_3\rangle \langle \psi_3| \\ & + \rho_{44}^s |\psi_4\rangle \langle \psi_4| + \rho_{23}^s e^{-ik_0 r_{12} \cos\theta} |\psi_2\rangle \langle \psi_3| \\ & + \rho_{32}^s e^{ik_0 r_{12} \cos\theta} |\psi_3\rangle \langle \psi_2|, \end{aligned} \quad (9)$$

where $\rho_{ij}^s = \langle i_A | \rho^s | j_A \rangle$ are the steady-state populations in dressed two-atom collective representation for $i = j$ and the interatomic coherences for $i \neq j$. The parameter θ carried by the coherences is the azimuthal angle of the detector from the interatomic axis. The explicit expressions of ρ_{ij}^s are presented in Appendix A. In Eq. (9), the state functions $|\psi_i\rangle$ triggered by the initial atomic states $|i_A\rangle$ are found as

$$\begin{aligned} |\psi_1\rangle = & C_{1,0}^{(1)} |1_A, 0_a\rangle + C_{2,0}^{(1)} |2_A, 0_a\rangle + C_{3,0}^{(1)} |3_A, 0_a\rangle + C_{4,1}^{(1)} |1_A, 1_a\rangle \\ & + C_{2,1}^{(1)} |2_A, 1_a\rangle + C_{3,1}^{(1)} |3_A, 1_a\rangle + C_{4,1}^{(1)} |4_A, 1_a\rangle, \\ |\psi_2\rangle = & C_{1,0}^{(2)} |1_A, 0_a\rangle + C_{2,0}^{(2)} |2_A, 0_a\rangle + C_{4,0}^{(2)} |4_A, 0_a\rangle \\ & + C_{1,1}^{(2)} |1_A, 1_a\rangle + C_{2,1}^{(2)} |2_A, 1_a\rangle \\ & + C_{3,1}^{(2)} |3_A, 1_a\rangle + C_{4,1}^{(2)} |4_A, 1_a\rangle, \end{aligned}$$

$$\begin{aligned} |\psi_3\rangle = & C_{3,0}^{(3)} |3_A, 0_a\rangle + C_{4,0}^{(3)} |4_A, 0_a\rangle \\ & + C_{3,1}^{(3)} |3_A, 1_a\rangle + C_{4,1}^{(3)} |4_A, 1_a\rangle, \\ |\psi_4\rangle = & C_{3,0}^{(4)} |3_A, 0_a\rangle + C_{4,0}^{(4)} |4_A, 0_a\rangle \\ & + C_{3,1}^{(4)} |3_A, 1_a\rangle + C_{4,1}^{(4)} |4_A, 1_a\rangle. \end{aligned} \quad (10)$$

The explicit analytical expressions of all the conditional transition probability amplitudes appearing in Eq. (10) are given in Appendix B. Interestingly, their algebraic forms correspond obviously to the transition channels in the energy level diagrams shown in Fig. 2. In physical terms, $C_{j,n}^{(i)}$ ($i, j = 1, 2, 3, 4, n = 0, 1$) describe the physical state that, before one of the photons is detected, the dressed collective atom has completed the single-photon emission or the two-photon cascaded emission triggered from the initial atomic state $|i_A\rangle$. After a probe, the atom is collapsed to the intermediate state $|j_A\rangle$ of two-photon cascaded path without leaving a photon in the cavity ($|0_a\rangle$), or collapsed to the final state $|j_A\rangle$ of two-photon cascaded path, remaining the second photon in the cavity ($|1_a\rangle$). Based on this understanding and the explicit forms of the conditional transition probability amplitudes in Appendix B, all the probability amplitudes involving probing another photon conditioned on the first detection stem from the quantum interference of two two-photon cascaded emission channels.

In this respect, in the above conditional state, only the probability amplitudes of single-photon state $|1_a\rangle$ contribute to the final conditional detection probability. Therefore, the unnormalized two-photon correlation signal $G^{(2)}$ can be obtained naturally, which is written compactly as

$$\begin{aligned} G^{(2)} = & \rho_{11}^s (|C_{1,1}^{(1)}|^2 + |C_{2,1}^{(1)}|^2 + |C_{3,1}^{(1)}|^2 + |C_{4,1}^{(1)}|^2) \\ & + \rho_{22}^s (|C_{1,1}^{(2)}|^2 + |C_{2,1}^{(2)}|^2 + |C_{3,1}^{(2)}|^2 + |C_{4,1}^{(2)}|^2) \\ & + \rho_{33}^s (|C_{3,1}^{(3)}|^2 + |C_{4,1}^{(3)}|^2) + \rho_{44}^s (|C_{3,1}^{(4)}|^2 + |C_{4,1}^{(4)}|^2) \\ & + 2 \text{Re}[\rho_{23}^s (C_{3,1}^{(2)} C_{3,1}^{(3)*} + C_{4,1}^{(2)} C_{4,1}^{(3)*}) e^{-ik_0 r_{12} \cos\theta}]. \end{aligned} \quad (11)$$

Ingeniously, it is the compact form of the conditional state in Eq. (9) expressed by the transition amplitudes that serves as the rudiment of the two-photon correlation given by Eq. (11). One can notice from Eq. (11) that both the correlation components determined by ρ_{11}^s and ρ_{22}^s consist of four terms. It represents that, conditioned on the detection of a photon, the another photon can be prepared at four different final atomic states, respectively, as depicted in Figs. 2(a) and 2(b). The conditional probability components determined by ρ_{33}^s and ρ_{44}^s are similar that both of them can prepare photons at final states $|3_A\rangle$ and $|4_A\rangle$, as depicted in Figs. 2(c) and 2(d). Whereas, the component involving ρ_{23}^s (with ρ_{32}^s) is created from the atomic coherence because two different initial states $|2_A\rangle$ and $|3_A\rangle$ can reach common final states $|3_A\rangle$ and $|4_A\rangle$.

Figure 3 presents the stationary atomic populations and interatomic coherence varying with the interatomic distance. The solid lines, dashed lines, and dotted-dashed lines represent the analytical results solved from the transformed equations (6), (7), and (8) with the help of the rotating-wave

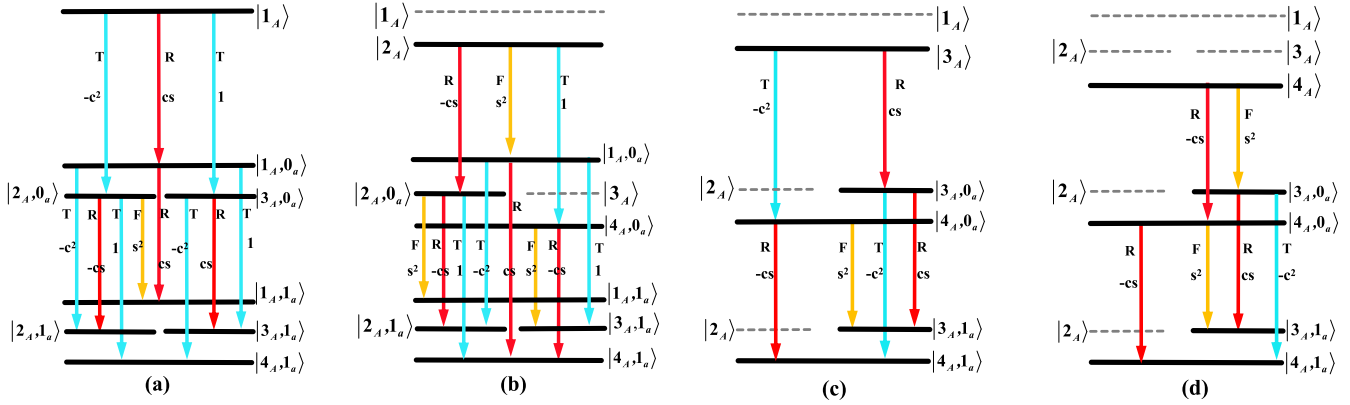


FIG. 2. Fluorescent emissions in dressed two-atom collective levels involving central peak labeled by R (red arrows), lower-frequency side peak labeled by F (yellow arrows), and higher-frequency side peak labeled by T (blue arrows) in resonance fluorescence spectrum. (a), (b), (c), and (d) correspond to all possible two-photon cascaded emissions triggered by the initial atomic states $|1_A\rangle$, $|2_A\rangle$, $|3_A\rangle$, and $|4_A\rangle$, respectively. The conditional states and single-photon bare (unfiltered) transition amplitudes are indicated.

approximation. At the same time, the circular lines are the corresponding numerical results from the original equations (1), (2), and (3). Obviously, only the populations ρ_{33}^s and ρ_{44}^s are dominant, which are mainly related to the host quantum radiating source. Whereas, ρ_{11}^s and ρ_{22}^s come from the guest atom, and make less contributions. Hence, let us concentrate on these two dominant populations in more detail. Based on the above analysis, it is natural to note that the components $\rho_{33}^s |C_{3,1}^{(3)}|^2$ and $\rho_{44}^s |C_{4,1}^{(4)}|^2$ in Eq. (11) should be grouped into the same physical consequence. Because it comes from the

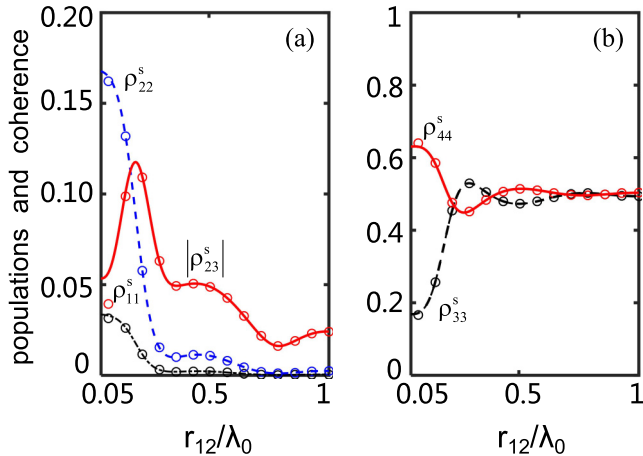


FIG. 3. Stationary populations and coherence of the dressed collective atom as functions of the interatomic distance r_{12} for the parameters $\kappa = 20\gamma$, $\Omega = 100\gamma$, $\Delta_2 = 0$, and $\Theta = \pi/4$. ρ_{11}^s (black dotted-dashed line and black circular line), ρ_{22}^s (blue dashed line and blue circular line), and $|\rho_{23}^s|$ (red solid line and red circular line) are plotted in (a). The dominant populations ρ_{33}^s (black dashed line and black circular line) and ρ_{44}^s (red solid line and red circular line) are plotted in (b). In each frame, the circular lines are the numerical results from the original equations (1), (2), and (3) without rotating-wave approximation, while the solid lines, dashed lines, and dotted-dashed line represent the analytical results solved from the transformed equations (6), (7), and (8) with the help of rotating-wave approximation.

quantum interference between the cascaded emissions of central peak photons ($|3_A\rangle \xrightarrow{R} |3_A\rangle \xrightarrow{R} |3_A\rangle$ for ρ_{33}^s and $|4_A\rangle \xrightarrow{R} |4_A\rangle \xrightarrow{R} |4_A\rangle$ for ρ_{44}^s) and the alternating cascaded emissions of two opposite sideband photons ($|3_A\rangle \xrightarrow{T} |4_A\rangle \xrightarrow{F} |3_A\rangle$ for ρ_{33}^s and $|4_A\rangle \xrightarrow{F} |3_A\rangle \xrightarrow{T} |4_A\rangle$ for ρ_{44}^s). Actually, these processes obey two-photon far-off-resonance condition when the cavity frequency is tuned to halfway between the central peak and a sideband. Therefore, it gives a very small probability. However, the component $\rho_{33}^s |C_{4,1}^{(3)}|^2$ is the product of the quantum interference of two two-photon cascaded channels involving R and T photons with opposite emission orderings, i.e., $|3_A\rangle \xrightarrow{T} |4_A\rangle \xrightarrow{R} |4_A\rangle$ and $|3_A\rangle \xrightarrow{R} |3_A\rangle \xrightarrow{T} |4_A\rangle$, as shown in Fig. 2(c). These two two-photon emissions interfered with each other are initiated from a common state $|3_A\rangle$ and terminated to a common state $|4_A\rangle$. Similarly, another term $\rho_{44}^s |C_{3,1}^{(4)}|^2$ is the consequence of the quantum interference of two two-photon cascaded channels involving R and F photons with opposite emission orderings, i.e., $|4_A\rangle \xrightarrow{R} |4_A\rangle \xrightarrow{F} |3_A\rangle$ and $|4_A\rangle \xrightarrow{F} |3_A\rangle \xrightarrow{R} |3_A\rangle$, as shown in Fig. 2(d). More significantly, there is a significant imbalance between these two parts when the cavity is tuned to halfway between the central peak and a certain side peak. For example, if the cavity frequency is tuned to halfway between the central peak and the higher-frequency side peak, i.e., $\Delta_c = \bar{\Omega}/2$, the R photons and T photons are injected into the cavity significantly, whereas the unidirectional radiations of F photons are almost prevented by the frequency window of the filter. Therefore, the probability component $\rho_{33}^s |C_{4,1}^{(3)}|^2$ can contribute a very large value accounting for the vast majority of the total value of $g^{(2)}$ [which can be seen in Fig. 4(a) later], and superbunching is displayed. Meanwhile, this case gives negligible probability of detecting the lower-frequency fluorescent radiations depicted by the yellow arrows in Fig. 2 because it is far from resonance with the target frequency. Symmetrically, if the cavity is tuned at $\Delta_c = -\bar{\Omega}/2$, the component $\rho_{44}^s |C_{3,1}^{(4)}|^2$ gives rise to a very large conditional probability component. Correspondingly, the unidirectional

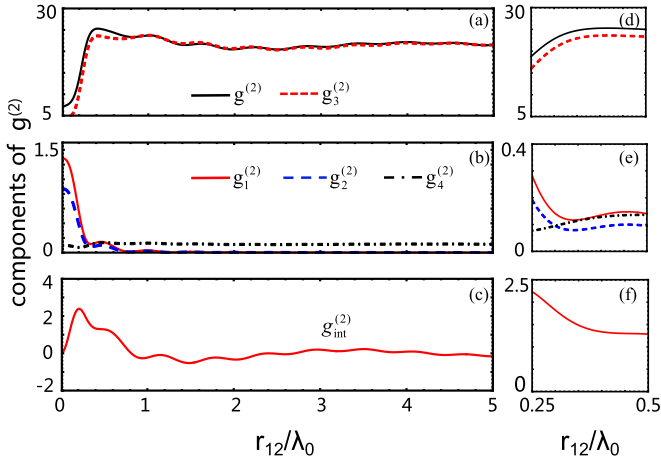


FIG. 4. The value of $g^{(2)}$ varying with the interatomic distance r_{12} is decomposed into some components $g_i^{(2)}$ ($i = 1, 2, 3, 4$) and $g_{\text{int}}^{(2)}$ in (a), (b), and (c), which are contributed from the steady populations ρ_{ii}^s and the interatomic coherences ρ_{23}^s (with ρ_{32}^s), respectively. (d), (e), and (f) are the enlarged views of (a), (b), and (c), respectively, for $r_{12} \in [0.25\lambda_0, 0.5\lambda_0]$. The parameters are $\kappa = 20\gamma$, $\Omega = 100\gamma$, $\Delta_2 = 0$, $\Theta = \pi/4$, and $\theta = \pi/4$.

radiations of higher-frequency fluorescent photons, depicted by the blue arrows in Fig. 2, are almost suppressed in this case.

Taking the case of $\Delta_c = \bar{\Omega}/2$ as the example and with the help of the introduced filtered transition amplitudes in Appendix B, this strong quantum correlation can be attributed to the constructive quantum interference between the coupled two-photon cascaded channels, namely, $|3_A\rangle \xrightarrow{T} |4_A\rangle \xrightarrow{R} |4_A\rangle$ and $|3_A\rangle \xrightarrow{R} |3_A\rangle \xrightarrow{T} |4_A\rangle$. Furthermore, this constructive quantum interference is the consequence of the fact that bare two-photon cascaded transition amplitudes c^3s and $-c^3s$, establishing destructive interference originally [10,12], are modified into the Lorentzian type. When the filter setting frequency approaches to halfway between the central peak and the higher-frequency side peak, these two bare two-photon transition amplitudes are modified to the greatest extent with opposite filtering detunings, making it possible that the complete destructive interference in bare is converted into the incomplete destructive interference, and finally into the constructive interference.

As a brief physical summary of the above discussions, we would like to stress the role of the filter-detector monitoring system. On the one hand, from the compact structure of the conditional state, the laser-dressed atomic system is prepared at the superposition states both for intermediate or final states. It means that the filter-detector system has no preferential selectivity for the spectral bands and transition channels in the situation of large detuning between the filter and the spectral peak. Thus, quantum interference is displayed between several paired two-photon cascaded channels coupled with each other via common initial states and final states. On the other hand, it is the effect of the filter on the monitored quantum radiating system by dressing the atom's unfiltered transition amplitudes into the Lorentzian type that makes it possible to export different photon statistics by frequency engineering.

IV. APPLICATIONS OF TWO-ATOM RADIATING SYSTEM

A. Single two-level atom limit

In addition to gaining the physical insight into the radiating mechanism in the above investigation, another superiority of the above analytical results is that it can be regressed into the Mollow limit of the single two-level atom algebraically. This case refers to the infinite interatomic distance. As shown in Fig. 3, with the increase of the interatomic distance, the collective atom can not be populated at $|1_A\rangle$ and $|2_A\rangle$ with the interatomic coherence ρ_{23} vanishing. Whereas, the remaining two states account for half of the total population for resonant driving, i.e., $\Delta_2 = 0$. The physical fact is that only the host atom is radiating and gives rise to an independent Mollow triplet. In this single-atom limit, the conditional state in Eq. (9) can be truncated as

$$\rho_0^r = \rho_{33}^{s(0)} |\psi_3\rangle\langle\psi_3| + \rho_{44}^{s(0)} |\psi_4\rangle\langle\psi_4|. \quad (12)$$

Therefore, the unnormalized two-photon correlation function in Eq. (11) is also simplified as

$$G_0^{(2)} = \rho_{33}^{s(0)} (|C_{3,1}^{(3)}|^2 + |C_{4,1}^{(3)}|^2) + \rho_{44}^{s(0)} (|C_{3,1}^{(4)}|^2 + |C_{4,1}^{(4)}|^2), \quad (13)$$

in which $\rho_{33}^{s(0)}$ and $\rho_{44}^{s(0)}$ are the populations of the single laser-dressed atom, which can be easily obtained from the collective atomic populations ρ_{33}^s and ρ_{44}^s when $\Omega_{12} = \gamma_{12} = 0$. The filtered fluorescent spectral correlation in single two-level atom has been developed systematically, especially concerning the time orderings [10,19]. As we expected, after straightforward algebraic arrangement, our analytical result given by Eq. (13) reproduces the analytical form calculated by the early fundamental method of two-photon detection operator established by Nienhuis *et al.* [10]. This verification can be found in Appendix C. Therefore, the strong quantum correlation discussed in the above can be traced back to the Mollow triplet of a single two-level atom. As reported in Ref. [17], this underlying photon statistics is a promising quantum excitation for applications, triggering a burgeoning field called ‘‘Mollow spectroscopy $_{\pm}$.’’ Its physical origin can also be understood as the leapfrog transitions involving virtual states [8,18]. Furthermore, this direct multiphoton cascaded emission jumping over the intermediate manifold can also display strong high-order quantum correlation [8]. Experimentally, this strong quantum correlation of filtered resonance fluorescence from a single two-level atom has been verified to violate the Cauchy-Schwarz inequality and Bell's inequality [21–23], which indicates that it is still a subject of current interest in quantum optics.

B. Enhancement of strong quantum correlation via interatomic coherence

Now, turning back to the two-atom radiating system under our consideration, an interesting question may arise naturally that, in the presence of the guest atom, whether the interatomic coherence can play an active role in breaking through the limit of the strong quantum correlation obtained from a single two-level atom under the same parametric conditions.

In order to track down the possible conditions analytically, let us still consider the two-photon correlation signal of the two-atom radiating system with large filter width. The value of $g^{(2)}$ is simultaneously dependent on the obtained unnormalized two-photon correlation $G^{(2)}$ and the steady filtered radiation intensity $G^{(1)} = \langle a^\dagger a \rangle$, which takes the form of [32]

$$G^{(1)} = \frac{\kappa\gamma c^2 s^2}{\left(\frac{\kappa}{2}\right)^2 + \Delta_c^2} + \frac{\kappa\gamma s^4(\rho_{22}^s + \rho_{44}^s)}{\left(\frac{\kappa}{2}\right)^2 + (\Delta_c + \bar{\Omega})^2} + \frac{\kappa\gamma c^4(\rho_{11}^s + \rho_{33}^s)}{\left(\frac{\kappa}{2}\right)^2 + (\Delta_c - \bar{\Omega})^2} + \frac{\kappa\gamma(\rho_{11}^s + \rho_{22}^s)}{\left(\frac{\kappa}{2}\right)^2 + (\Delta_c - \bar{\Omega})^2} - \frac{2\kappa\gamma c^2 \text{Re}[\rho_{23}^s e^{-ik_0 r_{12} \cos\theta}]}{\left(\frac{\kappa}{2}\right)^2 + (\Delta_c - \bar{\Omega})^2}. \quad (14)$$

It is straightforward to note that the total filtered radiation intensity can be decomposed into three parts. The first three terms together constitute the complete filtered emission spectrum of the laser-driven host atom. Clearly, it is very similar to the standard Mollow triplet, except that the linewidths are modified by the filter. The fourth term is the independent emission spectrum of the guest atom, which only radiates the higher-frequency fluorescence. Whereas, the last term of Eq. (14), which we shall call the ‘‘intensity interference component’’ labeled by $G_{\text{int}}^{(1)}$ in the following, is more worthy of our consideration. Because it exhibits the intensity interference of the fluorescent fields radiated from two quantum light sources, i.e., the host atom and the guest atom. More interestingly, it is not only determined by the internal interatomic coherence ρ_{23}^s , but also by the steerable geometrical factors r_{12} , Θ , and θ [32]. As depicted in Fig. 2, Eq. (14) also indicates that the lower-frequency spectral line proportional to the populations ρ_{22}^s and ρ_{44}^s results from the atomic downward transitions $|2_A\rangle \rightarrow |1_A\rangle$ and $|4_A\rangle \rightarrow |3_A\rangle$, respectively. Both of them come from the driven atom, with the undriven atom’s state unchanged. The intensity of higher-frequency spectral line is proportional to the populations ρ_{11}^s , ρ_{22}^s , ρ_{33}^s , and the interatomic coherence ρ_{23}^s . It corresponds to the four possible atomic downward transitions $|1_A\rangle \rightarrow |2_A\rangle$, $|1_A\rangle \rightarrow |3_A\rangle$, $|2_A\rangle \rightarrow |4_A\rangle$, and $|3_A\rangle \rightarrow |4_A\rangle$, in which the fluorescent photons from $|1_A\rangle \rightarrow |2_A\rangle$ and $|3_A\rangle \rightarrow |4_A\rangle$ are radiated from the driven atom, whereas the photons from $|1_A\rangle \rightarrow |3_A\rangle$ and $|2_A\rangle \rightarrow |4_A\rangle$ are radiated from the undriven atom. The central spectral line, however, is associated with all the populations with the atomic downward transitions between the same states of two adjacent manifolds of the dressed collective states. Both downward transitions of R photons originate from the driven atom.

Our strategy is to find some possible conditions for r_{12} and θ in an appropriate distance interval, in which the steady populations ρ_{11}^s , ρ_{22}^s , and ρ_{44}^s have less influence on the value of $g^{(2)}$. We intend to adjust the geometrical factors including the dipole-polarized angle Θ and detection angle θ to make the coherence play a full role in regulating the value of $g^{(2)}$. Therefore, taking an example that the cavity frequency is tuned to $\Delta_c = \bar{\Omega}/2$, let us search for the possible condition for r_{12} and θ from the intensity interference.

The intensity interference $G_{\text{int}}^{(1)}$ can be rewritten as

$$G_{\text{int}}^{(1)} = \frac{-2\kappa\gamma c^2}{\left(\frac{\kappa}{2}\right)^2 + \left(\frac{\bar{\Omega}}{2}\right)^2} |\rho_{32}^s| \cos\left(2\pi \frac{r_{12}}{\lambda_0} \cos\theta + \varphi_{32}\right), \quad (15)$$

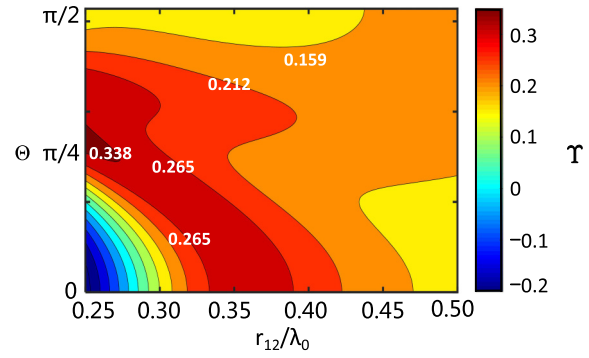


FIG. 5. Contour plot of Υ as a function of the dipole-polarized angle Θ and the interatomic distance r_{12} for $\kappa = 20\gamma$, in which the detection angle θ and the interatomic distance r_{12} satisfy the condition given by Eq. (16). Other parameters are $\Omega = 100\gamma$, $\Delta_2 = 0$. Optimal enhancement of $g^{(2)}$ corresponds to the red zone.

where φ_{32} is the phase angle of the atomic coherence, i.e., $\rho_{32}^s = |\rho_{32}^s| e^{i\varphi_{32}}$. This form suggests that a condition for enhancing the value of $g^{(2)}$ is possible if the total intensity is suppressed when r_{12} and θ satisfy the relation

$$\cos\theta = \frac{\lambda_0}{r_{12}} \left(m - \frac{\varphi_{32}}{2\pi}\right), \quad m \in \{0, \pm 1, \pm 2, \dots\}, \quad (16)$$

in which m is constrained by $\left(\frac{\varphi_{32}}{2\pi} - \frac{r_{12}}{\lambda_0}\right) \leq m \leq \left(\frac{\varphi_{32}}{2\pi} + \frac{r_{12}}{\lambda_0}\right)$.

For more clarity, the value of $g^{(2)}$ is decomposed in Fig. 4 for $\kappa = 20\gamma$, $\Omega = 100\gamma$, $\Delta_2 = 0$, $\Theta = \pi/4$, and $\theta = \pi/4$. In Fig. 4, $g_i^{(2)}$ are the components determined by the stationary populations ρ_{ii}^s , and $g_{\text{int}}^{(2)}$ is the normalized correlation interference component. All the components of $g^{(2)}$ are normalized by the total intensity, i.e., $g_1^{(2)} + g_2^{(2)} + g_3^{(2)} + g_4^{(2)} + g_{\text{int}}^{(2)} = g^{(2)}$. In order to compare with the single-atom case, the contributions from ρ_{11}^s and ρ_{22}^s should be minimized as far as possible, and only give full play to the interatomic coherence. Thus, the variation interval of r_{12} is temporarily set to be $[0.25\lambda_0, 0.5\lambda_0]$. In this interval, $m = 0$ is the only allowed value for the condition given by Eq. (16). In this interval, compared with the correlation component given by the interatomic coherence ρ_{23}^s , the contributions from the populations ρ_{11}^s and ρ_{22}^s are very small to the total value of $g^{(2)}$, as presented in Figs. 4(d), 4(e), and 4(f), which makes it possible to manipulate the values of $g^{(2)}$ by the interatomic coherence.

In order to compare with the superbunching in a single-atom limit quantitatively under the same parametric conditions, we introduce $\Upsilon = \Delta g^{(2)}/g_0^{(2)}$ to characterize the enhancing rate of the value of $g^{(2)}$. In this definition, $\Delta g^{(2)}$ is the deviation of $g^{(2)}$, i.e., $\Delta g^{(2)} = g^{(2)} - g_0^{(2)}$, with $g^{(2)}$ and $g_0^{(2)}$ being, respectively, the values of two-photon correlation function of the two-atom radiating system under our consideration and the single two-level atom, i.e., $\Omega_{12} = \gamma_{12} = 0$, under the same parameters. Figure 5 shows the variation of Υ with the dipole-polarized angle Θ and the interatomic distance r_{12} with the parameters $\Delta_2 = 0$, $\Omega = 100\gamma$, and $\kappa = 20\gamma$, while the detection angle θ is absorbed by r_{12} via Eq. (16). It can be observed that the superbunching effect can be improved for a larger range of Θ and r_{12} . Furthermore, the optimized value of Υ can reach 35% for $g^{(2)} \approx 29.06$ and $g_0^{(2)} \approx 21.52$ when

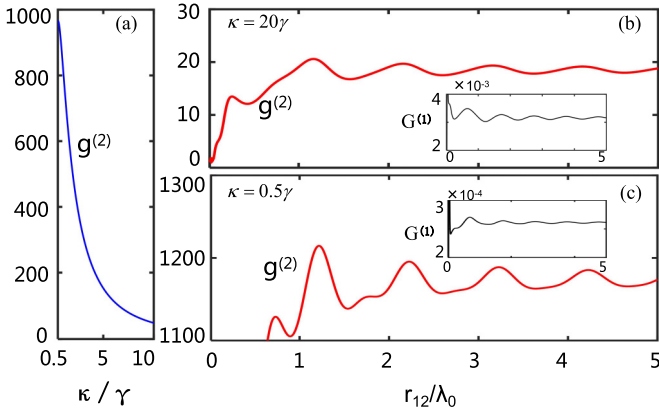


FIG. 6. (a) The value of $g^{(2)}$ as a function of the cavity dissipation rate κ for $\Omega = 100\gamma$, $\Delta_2 = 0$, $\Theta = \pi/2$, $\theta = \pi/2$, and $r_{12} = 0.25\lambda_0$. Normalized two-photon correlation $g^{(2)}$ as a function of the interatomic distance r_{12} for large filter width $\kappa = 20\gamma$ (b) and narrow filter width $\kappa = 0.5\gamma$ (c). Other parameters are $\Omega = 100\gamma$, $\Delta_2 = 0$, $\Theta = \pi/2$, and $\theta = \pi/2$. The filtered radiation intensities in these two case are inserted in (b) and (c), respectively.

$r_{12} = 0.25\lambda_0$ and the atomic dipole moments are polarized at $\Theta \approx 0.85$. Under these parameters, two appropriate observation angles $\theta_1 = 1.9$ and $\theta_2 = 2\pi - \theta_1 = 4.38$ can be determined corresponding to the minimum value of the filtered radiation intensity. Fortunately, some reports have provided the experimental feasibility of trapping the atoms with the fixed atomic dipole moment and locations [43–46]. Our result demonstrates that although a very significant superbunching may not be achieved in the case of large filter width, the superbunching limit in single-atom Mollow triplet can be still broken with the help of the interatomic coherence in this two-atom radiating system.

C. Precise detection of interatomic distance

As another application of the two-atom radiating system we are considering, here we briefly discuss the feasibility of precisely detecting the variation of the interatomic distance via this superbunched fluorescent photon generated from this interesting frequency.

Figure 6(a) presents the value of $g^{(2)}$ as a function of the cavity dissipation rate κ when its frequency is tuned to the middle of the R peak and T peak. It indicates that the degree of the superbunching effect increases sharply as the cavity develops from a broadband filter to a narrow-band filter. The main reason is understandable. For a filter with narrow width, in order to select photons with high-accuracy target frequency, the resolving time of the filter, i.e., the reciprocal of the filter width, should be prolonged [8]. It is equivalent to a very long lifetime of photons in the cavity. Therefore, the coherence between the incident photons will be significantly improved. Although the photon number detected is greatly reduced in this case, the conditional probability can be significantly amplified. In other words, once a photon is detected, another photon will be detected with great probability.

The values of $g^{(2)}$ varying with the interatomic distance r_{12} are also presented for the case of large filter width with $\kappa = 20\gamma$ in Fig. 6(b) and narrow filter width with $\kappa = 0.5\gamma$

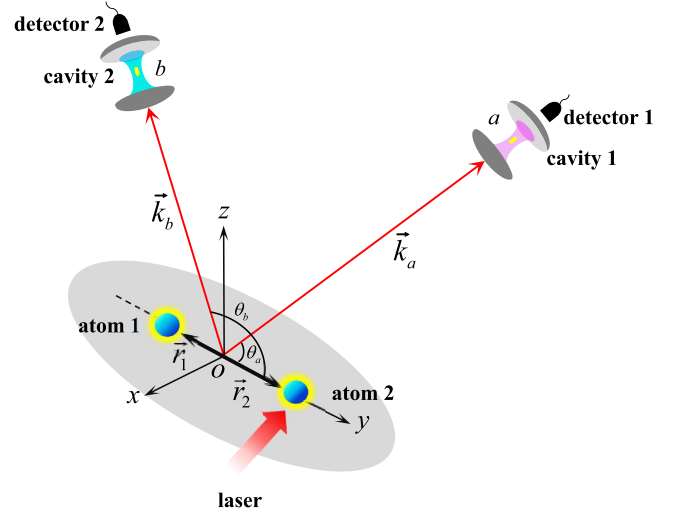


FIG. 7. Schematic diagram of a generalized cascaded quantum system. The two-atom radiating source is monitored by two detectors at two different geometrical points. Two single-mode cavities are applied in front of the two detectors to resolve the fluorescent photons with target frequency. The different observation directions of the two detectors are characterized by the azimuth angles θ_a and θ_b , and the corresponding propagation vectors \vec{k}_a , \vec{k}_b of the target fluorescent photons.

in Fig. 6(c), respectively. It can be observed that, with the variation of the interatomic distance, the deviation of the two-photon correlation signal outputted from a narrow-band filter is more significant than that in the case of the broadband filter in the same parameter regime, although the signal detected from the broadband filter is also able to clearly reflect the weak variation of the distance. However, in contrast, the outputted filtered radiation intensity seems powerless in this application, which can be observed from the intensity signals inserted in Figs. 6(b) and 6(c).

V. STRONG QUANTUM CORRELATION MONITORED BY TWO FILTER-DETECTOR SYSTEMS

In this section, we generalize our cascaded quantum system discussed in the above to the case of two filter-detector monitoring systems with the purpose of investigating the directionality of the filtered strongly correlated photon pairs.

As sketched in Fig. 7, in this generalized system, two photodetectors labeled by 1 and 2 are located at two different positions \vec{R}_1 and \vec{R}_2 , respectively, to simultaneously monitoring the filtered fluorescent photons. Two single-mode empty cavities are applied in front of them, respectively, to resolve the fluorescent photons radiated from the two-atom system. Due to the different azimuth angles θ_a and θ_b of the two filter-detector monitoring systems, the radiating directions of the fluorescent photons monitored by detector 1 and detector 2 are identified by their respective propagation vectors \vec{k}_a and \vec{k}_b . The corresponding quantum cavity fields in cavity 1 and cavity 2 are labeled as mode a and mode b , respectively.

Suppose that the condition of higher-frequency sideband resonance between the two atoms is still satisfied. Therefore,

the master equation of the generalized total quantum cascaded system in the dressed two-atom collective representation is the same as that in the case of a single filter, except for including two cavity fields in the Hamiltonian of Eq. (7) and the cavity dissipations of Eq. (8). In addition, the atom-cavity unidirectional dissipative coupling $\tilde{\mathcal{L}}_{AC}\rho$ in Eq. (8) should be generalized as

$$\begin{aligned} \tilde{\mathcal{L}}_{AC}\rho = & - \sum_{c=a,b} \sqrt{\kappa_c} \gamma_1 ([c^\dagger, S_1^- \rho] e^{i\vec{k}_c \cdot \vec{r}_1} + \text{H.c.}) \\ & - \sum_{c=a,b} \sum_{j=F,R,T} \sqrt{\kappa_c} \gamma_2 ([c^\dagger, S_j^- \rho] e^{i\vec{k}_c \cdot \vec{r}_2} + \text{H.c.}), \end{aligned} \quad (17)$$

where κ_a and κ_b are the decay rates of the cavity 1 and cavity 2, respectively. Based on the same analytical process of conditional detection as before, the normalized two-mode filtered fluorescent correlation signal

$$g_{ab}^{(2)}(\vec{R}_1, \vec{R}_2) = \frac{\langle a^\dagger b^\dagger ba \rangle}{\langle a^\dagger a \rangle \langle b^\dagger b \rangle} \quad (18)$$

can be calculated straightforwardly. For the sake of simplicity, we assume that the decay rates of the cavity fields $\kappa_a = \kappa_b = \kappa$, and the cavity frequencies $\Delta_{ca} = \Delta_{cb} = \Delta_c$. Then, the unnormalized two-photon correlation $G_{ab}^{(2)}(\vec{R}_1, \vec{R}_2) = \langle a^\dagger b^\dagger ba \rangle$ filtered by the two cavities is generalized as

$$\begin{aligned} G_{ab}^{(2)}(\vec{R}_1, \vec{R}_2) = & \rho_{11}^s [|C_{1,1}^{(1)}|^2 + |C_{2,1}^{(1)}|^2 + \eta(\theta_a, \theta_b) (|C_{3,1}^{(1)}|^2 + |C_{4,1}^{(1)}|^2)] \\ & + \rho_{22}^s [|C_{1,1}^{(2)}|^2 + |C_{2,1}^{(2)}|^2 + \eta(\theta_a, \theta_b) (|C_{3,1}^{(2)}|^2 + |C_{4,1}^{(2)}|^2)] \\ & + \rho_{33}^s (|C_{3,1}^{(3)}|^2 + |C_{4,1}^{(3)}|^2) + \rho_{44}^s (|C_{3,1}^{(4)}|^2 + |C_{4,1}^{(4)}|^2) \\ & + 2 \text{Re} [\rho_{23}^s (C_{3,1}^{(2)} C_{3,1}^{(3)*} + C_{4,1}^{(2)} C_{4,1}^{(3)*}) \xi(\theta_a, \theta_b)], \end{aligned} \quad (19)$$

with the spatial geometrical factors

$$\begin{aligned} \eta(\theta_a, \theta_b) = & \frac{1}{2} \{ 1 + \cos[k_0 r_{12} (\cos \theta_a - \cos \theta_b)] \}, \\ \xi(\theta_a, \theta_b) = & \frac{1}{2} (e^{-ik_0 r_{12} \cos \theta_a} + e^{-ik_0 r_{12} \cos \theta_b}). \end{aligned} \quad (20)$$

Clearly, it can be checked that if two cavity-detector monitoring systems overlap at the same geometrical point, i.e., $\theta_a = \theta_b = \theta$, $\vec{R}_1 = \vec{R}_2 = \vec{R}$, then the introduced geometrical factors are simplified as $\eta(\theta_a, \theta_b) = 1$ and $\xi(\theta_a, \theta_b) = e^{-ik_0 r_{12} \cos \theta}$. Therefore, the generalized unnormalized two-mode correlation $G_{ab}^{(2)}(\vec{R}_1, \vec{R}_2)$ reproduces the obtained result in Eq. (11). In addition, compared with Eq. (14), the stationary filtered radiation intensity of mode a (or mode b), i.e., $\langle a^\dagger a \rangle$ (or $\langle b^\dagger b \rangle$), does not need to be changed, just the detection angle θ should be concretized into θ_a (or θ_b).

From this generalized analytical result given by Eq. (19), it is worthwhile to discuss the physical origin of the geometrical factors. One can notice that, in addition to the two-photon correlation interference term being dependent on the geometric factor $\xi(\theta_a, \theta_b)$, there are also four probability components that are modulated by the spatial geometry $\eta(\theta_a, \theta_b)$. This geometrical factor originates from the quantum interference when two atoms alternately emit photons in different emission orderings. For example, the probability

amplitude $C_{3,1}^{(1)}$ corresponds to the quantum interference between two alternative two-photon cascaded emissions with opposite emission orderings, namely, via $|1_A\rangle \xrightarrow{R} |1_A\rangle \xrightarrow{T} |3_A\rangle$ and $|1_A\rangle \xrightarrow{T} |3_A\rangle \xrightarrow{R} |3_A\rangle$. In each two-photon emission orderings, the fluorescent photons R and T are radiated from the driven atom and the undriven atom, respectively. Thus, two opposite emission orderings of two atoms exhibit quantum interference modulated by the geometry. However, other terms independent of the geometrical factors represent the processes in which both the two photons emitted successively come from the same atom. It is not difficult to notice that the two processes in which two atoms alternately emit photons in opposite emission orderings can be interfered destructively when $\eta(\theta_a, \theta_b) = 0$, and we obtain

$$\cos \theta_a - \cos \theta_b = \left(m + \frac{1}{2} \right) \frac{\lambda_0}{r_{12}}, \quad m \in \{0, \pm 1, \pm 2, \dots\}. \quad (21)$$

Correspondingly, the condition of constructive quantum interference corresponding to the maximum geometrical modulation is given by $\eta(\theta_a, \theta_b) = 1$, which gives the condition of

$$\cos \theta_a - \cos \theta_b = m \frac{\lambda_0}{r_{12}}, \quad m \in \{0, \pm 1, \pm 2, \dots\}. \quad (22)$$

Since the geometrical factor appears in the undominant populations ρ_{11}^s and ρ_{22}^s , this geometrical modulation effect will disappear with the increase of the interatomic distance. Therefore, we specify the interatomic distance as $r_{12} = 0.25\lambda_0$. In this case, $\eta(\theta_a, \theta_b) = 0$ when $\theta_a = 0$, $\theta_b = \pi$, or $\theta_a = \pi$, $\theta_b = 0$, as depicted by the red arrows in Fig. 8(a). This also means that two possible processes of two-atom alternating radiation are interfered destructively when the two atoms radiate photons along the interatomic axis in the opposite directions. However, the constructive quantum interference of two photons radiated from two atoms, respectively, is given by a simple relation $\cos \theta_a = \cos \theta_b$, i.e., $\theta_a = \theta_b$ or $\theta_a = 2\pi - \theta_b$, as depicted by the green arrows in Fig. 8(a). To describe the sensitivity of two-photon correlation to the geometrical modulation, we explore the difference of $g_{ab}^{(2)}$ between these two cases, i.e., $\Delta g_{ab}^{(2)} = g_{ab+}^{(2)} - g_{ab-}^{(2)}$, where $g_{ab+}^{(2)}$ and $g_{ab-}^{(2)}$ are the two-photon correlation in the cases of $\eta(\theta_a, \theta_b) = 1$ and $\eta(\theta_a, \theta_b) = 0$, respectively. Figure 8(b) displays the distribution of $\Delta g_{ab}^{(2)}$ with the dipole-polarized angle Θ and the detection angles $\theta_a = \theta$ with $\theta_b = 2\pi - \theta$. The maximum difference can reach $\Delta g_{ab}^{(2)} = 11.5$, corresponding to the direction in which the geometrical modulation has the most significant effect on the two-photon correlation.

We now turn to consider the spatial angular distribution of two-mode correlation in this generalized case. Since the filtered radiation intensity only depends on the corresponding detection angle, the filtered radiation intensities of mode a and mode b are spatially equivalent. Figure 8(c) presents the stationary filtered radiation intensity of cavity mode a for the corresponding detection angle θ_a and the dipole-polarized angle Θ with parameters $\Omega = 100\gamma$, $\kappa = 20\gamma$, $r_{12} = 0.25\lambda_0$. As we have demonstrated, $\Theta = 0.85$ is a possible appropriate value for optimal enhancement of $g_{ab}^{(2)}$, and it gives two special detection angles $\theta_{a1} = 1.9$ and $\theta_{a2} = 2\pi - \theta_{a1} = 4.38$

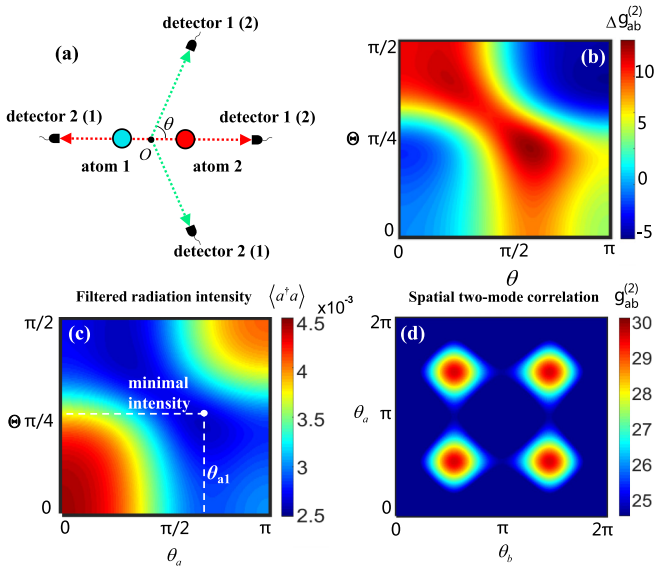


FIG. 8. (a) Possible detecting orientations for $\eta(\theta_a, \theta_b) = 0$ (red arrows) and $\eta(\theta_a, \theta_b) = 1$ (green arrows) when $r_{12} = 0.25\lambda_0$. (b) Distribution of $\Delta g_{ab}^{(2)}$ with the dipole-polarized angle Θ and detection angle $\theta_a = \theta$ ($\theta_b = 2\pi - \theta$) for $\Omega = 100\gamma$, $\Delta_2 = 0$, $\kappa_a = \kappa_b = 20\gamma$, $\Delta_a = \Delta_b = \bar{\Omega}/2$, and $r_{12} = 0.25\lambda_0$. (c) Filtered radiation intensity monitored by photodetector 1 as a function of its detection angle θ_a and the dipole-polarized angle Θ . When $\Theta = 0.85$, which may give rise to the optimal enhancement of $g_{ab}^{(2)}$, an appropriate observation angle corresponding to the minimum value of the filtered radiation intensity is $\theta_{a1} = 1.9$ labeled in the frame (c), i.e., the labeled point is $(\Theta = 0.85, \theta_{a1} = 1.9)$, and another possible angle $\theta_{a2} = 2\pi - \theta_{a1} = 4.38$ is not marked. (d) Two-dimensional angular distribution of the filtered two-photon correlation signal $g_{ab}^{(2)}(\theta_a, \theta_b)$ for $\Omega = 100\gamma$, $\Delta_2 = 0$, $\kappa_a = \kappa_b = 20\gamma$, $\Delta_a = \Delta_b = \bar{\Omega}/2$, $r_{12} = 0.25\lambda_0$, and $\Theta = 0.85$.

corresponding to the minimum value of $\langle a^\dagger a \rangle$. Therefore, the same is true for cavity mode b . Figure 8(d) presents the two-dimensional angular distribution of the normalized two-mode quantum correlation $g_{ab}^{(2)}(\theta_a, \theta_b)$. Four distinct peaks can be observed corresponding to $(\theta_{a1}, \theta_{b1})$, $(\theta_{a1}, \theta_{b2})$, $(\theta_{a2}, \theta_{b1})$, and $(\theta_{a2}, \theta_{b2})$, in which two peaks on the anti-diagonal line represent the simple case of a single filter. However, in addition to the case of single filter, this two-dimensional angular distribution suggests that the collective detection of two filter-detector systems located at two geometric points can provide more possible observation angle combinations $(\theta_{a1}, \theta_{b2})$ or $(\theta_{a2}, \theta_{b1})$ to realize directional strong quantum correlation. In other words, it refers to a fact that two filtered photons radiated from halfway between the central peak and a side peak are still highly correlated along these two special directions to break through the superbunching effect in the single-atom limit, even though they are spatially separated.

However, if one detector is applied to detect the filtered photons emitted along the atomic axis, the quantum correlation seems to have changed. For example, when only the detector 2 is located at $\theta_b = 0$ to achieve its maximum filtered radiation intensity under the given parameters, the value of two-mode quantum correlation is reduced, even if another detector 1 is still placed at two special angles, i.e.,

$\theta_1 = \theta_{a1}$ or θ_{a2} . This result can be attributed to the difference between the electric dipole operators of the collective atomic system coupled with two cavity modes along two different orientations, respectively. More specifically, the component of the electric dipole moments of the two atoms detected by the detector 1 at $\theta_a = \theta_{a1}$ exhibit in an opposite phase. This leads to the destructive interference of the radiation intensities $\langle a^\dagger a \rangle$ from the two quantum radiating sources. On the contrary, the filtered photons monitored by the detector 2 along the direction $\theta_b = 0$ are radiated from the two atoms whose electric dipole moments are in phase, which give rise to the maximum intensity of $\langle b^\dagger b \rangle$. This suggests that the counting rates of the two-atom system towards these two directions are different, which results in a reduction of the probability of simultaneously detecting two photons in different directions. Overall, however, the intrinsic superbunching effect can still be maintained regardless of these geometrical factors.

VI. CONCLUSION

In conclusion, the frequency-resolved photon correlation of resonance fluorescence has been investigated in a two-atom radiating system with the aim of exploring the underlying applications of the strong quantum correlation in this collective quantum system, including the enhancement of superbunching effect and precise detection for the weak variation of the interatomic distance. In addition, our analytical investigation makes it possible to probe into the physical mechanisms of the superbunching effect built up from halfway between the central band and one of the sidebands. In the case of large filter width, the conditional atom-photon state is studied in a truncated Hilbert space with single excitation for the cavity mode. The physical advantage of our approach lies in the fact that it can clearly present how the conditional state is developed into the two-photon correlation signal with evident analytical and physical correspondence. From our analytical formalism, the superbunching effect occurring between the central band and a sideband can be interpreted as the product of the constructive quantum interference between a pair of two-photon cascaded transitions, which is essentially the consequence of the modulation effect of the unfiltered transition amplitudes by the filter. As the second part of this paper, some applications of this two-atom radiating system have been also discussed. It has been shown that the interatomic coherence caused by the dipole-dipole interaction may play an active role in breaking through the superbunching limit obtained in an independent two-level atom. At the same time, it has been found that the strongly correlated photon pairs built up from this mechanism are robust to the weak variations of the interatomic distance. This suggests that, in addition to being a treasurable quantum pump, it can also serve as a promising quantum response to reflect this weak variation in the interior of the quantum radiating source itself. Finally, as the third part of this paper, we have generalized our investigation to the case of two filter-detector monitoring systems to explore the directionality of this superbunching effect. It has been found that this filtered strong quantum correlation can be also maintained even though the two photons are spatially separated and maximized at specific two-dimensional detection angle combinations. This preservation and directionality may

provide potential feasibility of engineering the filtered photon correlations in space.

ACKNOWLEDGMENTS

This work is supported by the National Natural Science Foundation of China (Grants No. 11774118 and No. 11474119) and the Fundamental Research Funds for the Central Universities of MOE (Grants No. CCNU18CXTD01 and No. CCNU17TS0006).

APPENDIX A: ANALYTICAL FORMS OF THE STATIONARY POPULATIONS AND ATOMIC COHERENCE

The coincidence of the stationary populations in dressed two-atom collective representation between the numerical solutions from the original master equations given by Eqs. (1), (2), and (3), and its analytical solutions from the transformed equations (6), (7), and (8), has been demonstrated in Sec. III. In this Appendix, we give the explicit analytical expressions of the dressed two-atom populations, which can clearly show the relationship between the two-atom system and the single two-level atom.

From Eqs. (6), (7), and (8), the steady-state populations in two-atom collective representation can be obtained straightforwardly, which are given by

$$\begin{aligned} \rho_{22}^s &= \frac{\chi_0 \chi_1}{\chi_3 \chi_4 - \chi_1 \chi_2}, & \rho_{33}^s &= \frac{\chi_0 \chi_4}{\chi_3 \chi_4 - \chi_1 \chi_2}, \\ \rho_{11}^s &= \frac{\chi_0 \chi_1 \gamma_-}{(\chi_3 \chi_4 - \chi_1 \chi_2)(\gamma_1 + \gamma_+)}, \end{aligned} \quad (\text{A1})$$

with the closed relation $\rho_{44}^s = 1 - \rho_{11}^s - \rho_{22}^s - \rho_{33}^s$. Whereas, only the atomic coherence ρ_{23}^s is nonzero, which is given by

$$\rho_{23}^s = \frac{-\tilde{\gamma}_{12}(2\rho_{11}^s - \rho_{22}^s - \rho_{33}^s) - 2ic^2\Omega_{12}(\rho_{22}^s - \rho_{33}^s)}{\gamma_1 + \gamma_+ + \gamma_- + 4\gamma_0}. \quad (\text{A2})$$

In the above solutions, the related coefficients are defined as

$$\begin{aligned} \chi_0 &= \gamma_-(\gamma_1 + \gamma_+)(\gamma_1 + \gamma_+ + \gamma_- + 4\gamma_0), \\ \chi_1 &= (\gamma_1 + \gamma_+)(\tilde{\gamma}_{12}^2 + 4c^4\Omega_{12}^2), \\ \chi_2 &= -\gamma_-(\gamma_+ + \gamma_-)(\gamma_1 + \gamma_+ + \gamma_- + 4\gamma_0) \\ &\quad - \tilde{\gamma}_{12}^2(2\gamma_- - \gamma_1 - \gamma_+) + 4c^4\Omega_{12}^2(\gamma_1 + \gamma_+), \\ \chi_3 &= (\gamma_1 + \gamma_+)(\gamma_+ + \gamma_-)(\gamma_1 + \gamma_+ + \gamma_- + 4\gamma_0) \\ &\quad + (\gamma_1 + \gamma_+)(4c^4\Omega_{12}^2 - \tilde{\gamma}_{12}^2), \\ \chi_4 &= \gamma_1(\gamma_1 + \gamma_+ + \gamma_-)(\gamma_1 + \gamma_+ + \gamma_- + 4\gamma_0) \\ &\quad + \tilde{\gamma}_{12}^2(2\gamma_- - \gamma_1 - \gamma_+) + 4c^4\Omega_{12}^2(\gamma_1 + \gamma_+), \end{aligned} \quad (\text{A3})$$

where the dressed-state transition rates are given by $\gamma_+ = \gamma_2 c^4$, $\gamma_- = \gamma_2 s^4$, $\gamma_0 = \gamma_2 c^2 s^2$, and $\tilde{\gamma}_{12} = \gamma_{12} c^2$. In addition, it can be examined straightforwardly that when $\Omega_{12} \rightarrow 0$ and $\gamma_{12} \rightarrow 0$, both the populations ρ_{11}^s , ρ_{22}^s and coherence ρ_{23}^s approach to zero, and the dominant populations are simplified as $\rho_{33}^{s(0)} = \frac{s^4}{c^4 + s^4}$ and $\rho_{44}^{s(0)} = \frac{c^4}{c^4 + s^4}$. This is the simple result of an independent laser-dressed two-level atom, i.e., the major quantum radiating source in the two-atom system under our consideration.

APPENDIX B: ANALYTICAL FORMS OF THE FILTERED TRANSITION AMPLITUDES IN EQ. (10)

In this Appendix, we give the explicit analytical forms of the filtered transition amplitudes in Eq. (10). In order to express these amplitudes with physically transparent forms, let us introduce the following single-photon filtered transition amplitudes for the filtered fluorescent photons from R peak, T peak, and F peak, respectively, as

$$\begin{aligned} C_{\text{R}}^+ &= \frac{cs\sqrt{\kappa\gamma}}{\frac{\kappa}{2} + i\Delta_c}, & C_{\text{R}}^- &= \frac{-cs\sqrt{\kappa\gamma}}{\frac{\kappa}{2} + i\Delta_c}, & C_{\text{T}}^+ &= \frac{\sqrt{\kappa\gamma}}{\frac{\kappa}{2} + i(\Delta_c - \bar{\Omega})}, \\ C_{\text{T}}^- &= \frac{-c^2\sqrt{\kappa\gamma}}{\frac{\kappa}{2} + i(\Delta_c - \bar{\Omega})}, & C_{\text{F}} &= \frac{s^2\sqrt{\kappa\gamma}}{\frac{\kappa}{2} + i(\Delta_c + \bar{\Omega})}. \end{aligned} \quad (\text{B1})$$

Actually, these forms are understandable. Due to the fact that the laser-dressed atom has two possible channels to give rise to the R peak in Mollow triplet, we use C_{R}^+ and C_{R}^- to distinguish these two different transitions with unfiltered amplitudes cs and $-cs$, respectively. Similarly, the radiation of T peak is built up from two channels, the undriven atom's transition and the laser-dressed atom's transition, with unfiltered amplitudes 1 and $-c^2$, respectively. Therefore, we use C_{T}^+ and C_{T}^- to express their filtered forms, respectively. The F peak corresponds to the isolated transition from the dressed atom with unfiltered amplitudes s^2 . Therefore, its filtered amplitude is labeled by C_{F} . It is apparent from Eq. (B1) that the filter, i.e., the target cavity, modulates the bare (or unfiltered) transition amplitudes of single fluorescent photon into Lorentzian type through dissipative coupling strength $\sqrt{\kappa\gamma}$. In terms of these definitions, all the probability amplitudes appearing in Eq. (10) can be completely determined as follows:

$$\begin{aligned} C_{1,0}^{(1)} &= C_{3,0}^{(3)} = C_{\text{R}}^+, & C_{2,0}^{(2)} &= C_{4,0}^{(4)} = C_{\text{R}}^-, \\ C_{3,0}^{(1)} &= C_{4,0}^{(2)} = C_{\text{T}}^+, & C_{2,0}^{(1)} &= C_{4,0}^{(3)} = C_{\text{T}}^-, \\ C_{1,0}^{(2)} &= C_{3,0}^{(4)} = C_{\text{F}}, \\ C_{1,1}^{(1)} &= C_{3,1}^{(3)} = \frac{-\sqrt{\kappa\gamma}}{\frac{\kappa}{2} + i\Delta_c}(csC_{\text{R}}^+ + s^2C_{\text{T}}^-), \\ C_{2,1}^{(2)} &= C_{4,1}^{(4)} = \frac{-\sqrt{\kappa\gamma}}{\frac{\kappa}{2} + i\Delta_c}(-c^2C_{\text{F}} - csC_{\text{R}}^-), \\ C_{2,1}^{(1)} &= C_{4,1}^{(3)} = \frac{-\sqrt{\kappa\gamma}}{\frac{\kappa}{2} + i(\Delta_c - \frac{\bar{\Omega}}{2})}(-c^2C_{\text{R}}^+ - csC_{\text{T}}^-), \\ C_{1,1}^{(2)} &= C_{3,1}^{(4)} = \frac{-\sqrt{\kappa\gamma}}{\frac{\kappa}{2} + i(\Delta_c + \frac{\bar{\Omega}}{2})}(s^2C_{\text{R}}^- + csC_{\text{F}}), \\ C_{3,1}^{(1)} &= \frac{-\sqrt{\kappa\gamma}}{\frac{\kappa}{2} + i(\Delta_c - \frac{\bar{\Omega}}{2})}(C_{\text{R}}^+ + csC_{\text{T}}^+), \\ C_{4,1}^{(1)} &= \frac{-\sqrt{\kappa\gamma}}{\frac{\kappa}{2} + i(\Delta_c - \bar{\Omega})}(C_{\text{T}}^- - c^2C_{\text{T}}^+), \\ C_{3,1}^{(2)} &= \frac{-\sqrt{\kappa\gamma}}{\frac{\kappa}{2} + i\Delta_c}(C_{\text{F}} + s^2C_{\text{T}}^+), \\ C_{4,1}^{(2)} &= \frac{-\sqrt{\kappa\gamma}}{\frac{\kappa}{2} + i\Delta_c - \frac{\bar{\Omega}}{2}}(C_{\text{R}}^- - csC_{\text{T}}^+). \end{aligned} \quad (\text{B2})$$

Obviously, all the conditional single-photon filtered amplitudes are originated from the quantum interference between different two-photon cascaded channels, and the algebraic forms of these filtered transition amplitudes can correspond exactly to the cascaded transition channels depicted in the energy level diagrams, as shown in Fig. 2.

APPENDIX C: FILTERED TWO-PHOTON CORRELATION IN SINGLE-ATOM LIMIT

In this Appendix, we verify the equivalence between our result of single-atom limit and the results in the existing literatures in terms of both analytical and numerical aspects. The unnormalized filtered two-photon correlation of the single-atom limit can also be calculated straightforwardly by the fundamental analytical method of the two-photon temporal detection operators proposed by Nienhuis *et al.* [10]. According to the spirit of this fundamental method, the unnormalized two-photon correlation can be expressed as $G_0^{(2)} = (F^\dagger F)$, in which F is the two-photon temporal detection operator. If all the spectral peaks are taken into account, the two-photon temporal detection operator should be generalized from the specific case of resonant detection discussed in Ref. [10]. The general form of F is expressed as

$$F = C_{FR}S_F^-S_R^- + C_{FT}S_F^-S_T^- + C_{RF}S_R^-S_F^- + C_{RR}S_R^-S_R^- + C_{RT}S_R^-S_T^- + C_{TF}S_T^-S_F^- + C_{TR}S_T^-S_R^-, \quad (C1)$$

in which the two-photon collective emission operators $S_\alpha^-S_\beta^-$ ($\alpha, \beta = F, R, T$) express that the atom radiates a β photon before the α photon is radiated. Therefore, the corresponding coefficients $C_{\alpha\beta}$ can be understood as the two-photon temporal emission amplitudes, which turn out to be

$$C_{FR} = \frac{\lambda^2}{(\lambda + i\Delta_c)[\lambda + i(\Delta_c + \frac{\Omega}{2})]},$$

$$C_{FT} = \frac{\lambda^2}{[\lambda + i(\Delta_c - \bar{\Omega})](\lambda + i\Delta_c)},$$

$$C_{RF} = \frac{\lambda^2}{[\lambda + i(\Delta_c + \bar{\Omega})][\lambda + i(\Delta_c + \frac{\Omega}{2})]},$$

$$C_{RT} = \frac{\lambda^2}{[\lambda + i(\Delta_c - \bar{\Omega})][\lambda + i(\Delta_c - \frac{\Omega}{2})]},$$

$$C_{TF} = \frac{\lambda^2}{[\lambda + i(\Delta_c + \bar{\Omega})](\lambda + i\Delta_c)},$$

$$C_{TR} = \frac{\lambda^2}{(\lambda + i\Delta_c)[\lambda + i(\Delta_c - \frac{\Omega}{2})]},$$

$$C_{RR} = \frac{\lambda^2}{(\lambda + i\Delta_c)^2}, \quad (C2)$$

with λ being the filter width. With this two-photon temporal emission operator, we get the result

$$G_0^{(2)} = \rho_{33}^{s(0)}(c^2s^2|C_{FT} - C_{RR}|^2 + c^3s|C_{RT} - C_{TR}|^2) + \rho_{44}^{s(0)}(c^3s|C_{FR} - C_{RF}|^2 + c^2s^2|C_{RR} - C_{TF}|^2). \quad (C3)$$

So far, we have quantitatively demonstrated that our result in single-atom limit given by Eq. (13) is completely equivalent to Eq. (C3) obtained from the fundamental method for frequency-resolved fluorescent spectral correlations with the time orderings being taken into account. The only difference between Eqs. (13) and (C3) is the scaling factor. The scaling factor in Eq. (13) is $\kappa^2\gamma^2$, while that of the latter is λ^4 . However, these factors can be canceled algebraically after normalization by the filtered radiation intensity.

On the other hand, the values of $g^{(2)}$ calculated numerically from the cascaded quantum system under our consideration have been verified by comparing it with the given experimental results. For example, according to Ref. [22], we chose the parameters $\gamma = 0.2$, $\Delta_2 = -1$, $\kappa = 0.5$, and $\Omega = 1.6$. Under these parameters, the cascaded approach in our consideration gives the two-photon correlation signal $g^{(2)} \approx 5.4$ for $\Delta_c = -\bar{\Omega}/2$ and $g^{(2)} \approx 4.4$ for $\Delta_c = \bar{\Omega}/2$, which basically agree with the experimental results in Ref. [22].

-
- [1] A. Ulhaq, S. Weiler, S. M. Ulrich, R. Roßbach, M. Jetter, and P. Michler, *Nat. Photonics* **6**, 238 (2012).
- [2] S. L. Portalupi, M. Widmann, C. Nawrath, M. Jetter, P. Michler, J. Wrachtrup, and I. Gerhardt, *Nat. Commun.* **7**, 13632 (2016).
- [3] F. P. Laussy, *Nat. Mater.* **16**, 398 (2017).
- [4] G. Bel and F. L. H. Brown, *Phys. Rev. Lett.* **102**, 018303 (2009).
- [5] A. González-Tudela, E. del Valle, and F. P. Laussy, *Phys. Rev. A* **91**, 043807 (2015).
- [6] C. S. Muñoz, F. P. Laussy, E. del Valle, C. Tejedor, and A. González-Tudela, *Optica* **5**, 14 (2018).
- [7] E. del Valle, *New J. Phys.* **15**, 025019 (2013).
- [8] A. Gonzalez-Tudela, F. P. Laussy, C. Tejedor, M. J. Hartmann, and E. del Valle, *New J. Phys.* **15**, 033036 (2013).
- [9] Y. Nieves and A. Muller, *Phys. Rev. B* **98**, 165432 (2018).
- [10] G. Nienhuis, *Phys. Rev. A* **47**, 510 (1993).
- [11] C. A. Schrama, G. Nienhuis, H. A. Dijkerman, C. Steijsiger, and H. G. M. Heideman, *Phys. Rev. A* **45**, 8045 (1992).
- [12] C. A. Schrama, G. Nienhuis, H. A. Dijkerman, C. Steijsiger, and H. G. M. Heideman, *Phys. Rev. Lett.* **67**, 2443 (1991).
- [13] S. Bounouar, M. Strauß, A. Carmele, P. Schnauber, A. Thoma, M. Gschrey, J.-H. Schulze, A. Strittmatter, S. Rodt, A. Knorr, and S. Reitzenstein, *Phys. Rev. Lett.* **118**, 233601 (2017).
- [14] A. Carmele, S. Bounouar, M. Strauß, S. Reitzenstein, and A. Knorr, *Phys. Rev. A* **99**, 023813 (2019).
- [15] J. C. López Carreño and F. P. Laussy, *Phys. Rev. A* **94**, 063825 (2016).
- [16] J. C. López Carreño, C. Sánchez Muñoz, E. del Valle, and F. P. Laussy, *Phys. Rev. A* **94**, 063826 (2016).
- [17] J. C. López Carreño, C. Sánchez Muñoz, D. Sanvitto, E. del Valle, and F. P. Laussy, *Phys. Rev. Lett.* **115**, 196402 (2015).
- [18] J. C. L. Carreño, E. del Valle, and F. P. Laussy, *Laser Photonics Rev.* **11**, 1700090 (2017).
- [19] V. N. Shatokhin and S. Y. Kilin, *Phys. Rev. A* **94**, 033835 (2016).

- [20] Q. Bin, Xin-You Lü, Li-Li Zheng, Shang-Wu Bin, and Ying Wu, *Phys. Rev. A* **97**, 043802 (2018).
- [21] C. Sánchez Muñoz, E. del Valle, C. Tejedor, and F. P. Laussy, *Phys. Rev. A* **90**, 052111 (2014).
- [22] M. Peiris, B. Petrak, K. Konthasinghe, Y. Yu, Z. C. Niu, and A. Muller, *Phys. Rev. B* **91**, 195125 (2015).
- [23] M. Peiris, K. Konthasinghe, and A. Muller, *Phys. Rev. Lett.* **118**, 030501 (2017).
- [24] H. F. Arnoldus and G. Nienhuis, *J. Phys. B: At. Mol. Phys.* **17**, 963 (1984).
- [25] J. H. Eberly and K. Wodkiewicz, *J. Opt. Soc. Am.* **67**, 1252 (1977).
- [26] J. D. Cresser, *J. Phys. B: At. Mol. Phys.* **20**, 4915 (1987).
- [27] E. del Valle, A. Gonzalez-Tudela, F. P. Laussy, C. Tejedor, and M. J. Hartmann, *Phys. Rev. Lett.* **109**, 183601 (2012).
- [28] K. Kamide, S. Iwamoto, and Y. Arakawa, *Phys. Rev. A* **92**, 033833 (2015).
- [29] C. W. Gardiner, *Phys. Rev. Lett.* **70**, 2269 (1993).
- [30] H. J. Carmichael, *Phys. Rev. Lett.* **70**, 2273 (1993).
- [31] K. Joosten and G. Nienhuis, *J. Opt. B* **2**, 158 (2000).
- [32] V. E. Lembessis, A. A. Rashed, O. M. Aldossary, and Z. Ficek, *Phys. Rev. A* **88**, 053814 (2013).
- [33] Z. Ficek and R. Tanaś, *Phys. Rep.* **372**, 369 (2002).
- [34] A. F. Alharbi and Z. Ficek, *Phys. Rev. A* **82**, 054103 (2010).
- [35] C. Cohen-Tannoudji and S. Reynaud, *Philos. Trans. R. Soc. London, Ser. A* **293**, 223 (1979).
- [36] V. N. Shatokhin and S. Y. Kilin, *Phys. Rev. A* **63**, 023803 (2001).
- [37] V. N. Shatokhin and S. Ya. Kilin, *Opt. Commun.* **174**, 157 (2000).
- [38] V. N. Shatokhin and S. Ya. Kilin, *Opt. Commun.* **210**, 291 (2002).
- [39] M. O. Scully and M. S. Zubairy, *Quantum Optics* (Cambridge University Press, Cambridge, UK, 1997).
- [40] G. S. Agarwal, *Springer Tracts in Modern Physics: Quantum Optics* (Springer, Berlin, 1974).
- [41] Z. Ficek and S. Swain, *Quantum Interference and Coherence: Theory and Experiments* (Springer, New York, 2005), Vol. 100.
- [42] J. S. Peng and G. X. Li, *Introduction to Modern Quantum Optics* (World Scientific, Singapore, 1998).
- [43] C. Langer, R. Ozeri, J. D. Jost, J. Chiaverini, B. DeMarco, A. Ben-Kish, R. B. Blakestad, J. Britton, D. B. Hume, W. M. Itano, D. Leibfried, R. Reichle, T. Rosenband, T. Schaetz, P. O. Schmidt, and D. J. Wineland, *Phys. Rev. Lett.* **95**, 060502 (2005).
- [44] D. Hayes, D. N. Matsukevich, P. Maunz, D. Hucul, Q. Quraishi, S. Olmschenk, W. Campbell, J. Mizrahi, C. Senko, and C. Monroe, *Phys. Rev. Lett.* **104**, 140501 (2010).
- [45] K. Kim, M. S. Chang, R. Islam, S. Korenblit, L. M. Duan, and C. Monroe, *Phys. Rev. Lett.* **103**, 120502 (2009).
- [46] D. B. Hume, C. W. Chou, T. Rosenband, and D. J. Wineland, *Phys. Rev. A* **80**, 052302 (2009).